Rotational Iron Losses in Brushless Doubly Fed Machines

S. Abdi, E. Abdi, *Senior Member, IEEE,* H. Toshani

***Abstract* – In this paper the rotational characteristics of the magnetic field in Brushless Double Fed Induction Machines (BDFIM) iron circuit is studied. The BDFIM has a complex magnetic field pattern which make its iron loss prediction difficult. This is due to the fact that BDFIM has two stator windings with different pole numbers which supply at different frequencies. In addition, the stator magnetic field contains excessive higher order field harmonics that make the conventional iron loss formulations not applicable to its iron loss predictions. A new iron loss formulation is proposed in this paper for the BDFIM that takes the rotational field and harmonic effects into account in the iron loss prediction. The proposed formulation is then verified using experimental tests on a prototype BDFIM with rotor open winding.**

***Index Terms*--Brushless doubly fed induction machine (BDFIM), Finite element (FE) analysis, Iron loss calculation, Rotational magnetic fields.**

I. Introduction

THE Brushless Doubly Fed Induction Machine (BDFIM) is an attractive electrical machine for wind drivetrain with a fractionally sized power converter at 30-35% of the generator rating, no brushes and slip rings on the rotor, and medium speed operation, making the gearbox system simplified compared to its high-speed counterpart i.e. Doubly Fed Induction Generator (DFIG) [1]. In addition, for variable speed drive applications requiring a moderate range of rotor speeds such as water pumps, BDFIM can be a cost-effective solution with lower capital and maintenance costs [2]. The BDFIM has also been appeared to be suited for small-scale hydropower due to the above technical and economic benefits [3].

The machine has a special design with two stator windings placed in common stator slots, and special rotor winding structures. The stator windings are designed with different pole numbers in a way that they do not couple directly with each other, the coupling is enabled by the rotor winding [4]. For standard operation, one stator winding is connected directly to the grid called the power winding (PW) and the other winding is supplied by an AC/AC power converter to provide variable voltage and variable frequency control, called the control winding (CW). Fig. 1 shows the BDFIM grid connection as a wind generator. There are several rotor winding structures proposed for the BDFIM, a well-known structure is the nested loop rotor [5], although other structures have shown to bring advantages in terms of both manufacturing and operation for large BDFIMs [6].

S. Abdi is with School of Engineering, University of East Anglia (UEA), Norwich, NR4 7TJ, UK (e-mail: s.abdi-jalebi@uea.ac.uk).

E. Abdi is with Wind Technologies Ltd, St. Johns Innovation Park, Cambridge, CB4 0WS, UK (e-mail: ehsan.abdi@windtechnologies.com).

H. Toshani is with CEPOWER Ltd, Cambridge, CB3 1AF, UK, and also with Department of Electrical Engineering, University of Cambridge, Cambridge, CB3 0FA, UK (e-mail: ht463@cam.ac.uk).

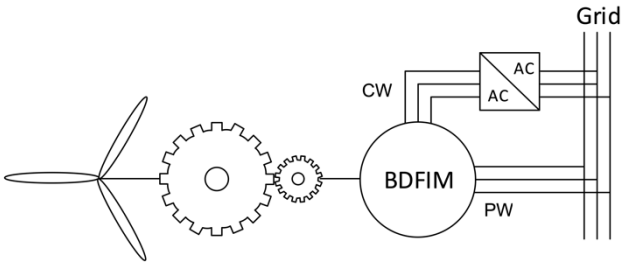

Fig. 1. A schematic of the BDFIM PW and CW grid connections.

Several experimental prototypes have been developed for the BDFM with the attempts to verify the machines' performance on large scale machines. These include the design and build of a 75 kW machine in Brazil [7], a 200 kW machine in China [8], 250 kW machine by the authors in the UK [9], and a 800 kW machine in China [10].

Due to the presence of two magnetic fields with different pole numbers and frequencies generated from the stator windings, the field pattern in the BDFIM's magnetic circuit is more complex than the conventional induction machines [11]. This makes the analysis and modelling of the BDFIM challenging. This is particularly the case when the iron loss modelling and prediction is concerned. There are several attempts for proposing iron loss predictions for the BDFIM.

In [12] the BDFIM was treated as a cascaded machine where the rotors of two induction machines with different pole numbers were electrically and mechanically connected. This was shown to be not effective for iron loss calculations especially when the stator hysteresis loss is to be analysed since the superposition principle cannot be applied due to the presence of hysteresis nonlinear effect.

In [13] the concepts of dissipation and restoring functions were studied in the BDFIM assuming that all the elements of iron losses in the stator and rotor iron can be considered separately, nevertheless the fact that the stator hysteresis loss from the two fields cannot be decoupled, was neglected.

Ferreira in [14] incorporated the iron loss model using the conventional equation with individual hysteresis, eddy current and excess loss components, in finite element (FE) analysis, and compared the calculated input power with measurements at the same operating conditions. However, the conventional iron loss model is based on the assumption that the machine's magnetic field distribution is sinusoidal and hence cannot be applied to the BDFIM with non-sinusoidal magnetic field pattern in its stator iron. Zhang et. al. [15] used a similar approach for iron loss calculation but also taking into account the rotational effects of the magnetic fields, however, no experimental iron loss measurement was reported.

Hashemnia et. al. [16] modified the BDFIM's equivalent circuit model by adding a parallel resistor representing the

iron loss effects in the steady state operation and hence improving the performance predictions. However, the discrepancy between simulation and experimental results remained evident, since the effects of the BDFM's special field in the calculation of stator hysteresis loss were ignored.

In all the above works on BDFIM iron loss analysis, there is no significant study on the rotational nature of the magnetic field in the BDFIM and how it should be included in the modelling of the machine's iron losses. The rotational variations of flux vectors in the core cause iron losses to increase compared with the situation in which there is only an alternating field. A higher rotational variation of the flux vectors leads to more iron losses.

In this paper special effort has been made to study the previous works on the iron loss calculations in the presence of rotational fields. The rotational nature of the BDFIM field in the stator and rotor iron is then broadly investigated using the finite element analysis. An iron loss prediction method based on a combination of an analytical and numerical FE approaches is proposed for the BDFIM taking the effects of the rotational fields into account in calculation of various iron loss components. The validity of the proposed methodology is finally assessed using experimental tests.

II. Magnetic Field Pattern in the BDFIM

The prototype BDFIM considered in this study is a D160 5.7 kW machine with the specifications provided in Table I. The synchronous mode is the desirable mode of operation for the BDFIM, where both stator windings are supplied. In this mode the BDFIM acts as a synchronous machine with the rotor rotating at a speed governed by the winding pole numbers and the mains and converter frequencies. The resultant magnetic field in synchronous mode will have a $p_1 + p_2$ pole configuration, where p_1 and p_2 are the PW and CW pole pair numbers, respectively [17].

The main difference with the induction machine's field is that the field strengths in a BDFIM for various poles are unequal at a time and those field strengths vary with time. For the prototype BDFIM considered in this study with 2 and 4 pole pair numbers for PW and CW, the air gap field has a 6-pole configuration as shown in Fig. 2. The above field characteristic results in a rotating magnetic field in the machine's iron with its pole fields pulsating with time.

TABLE I
Specifications of the prototype D160 BDFIM considered in this study

Frame size	D160	PW rated flux density	0.28 T
Stack length	190 mm	CW rated flux density	0.34 T
Lamination	M530-65A	Rated speed	700 rpm
PW pole pair number	2	PW rated voltage	415 V at 50 Hz
CW pole pair number	4	PW rated current	12 A
Stator number of slots	36	CW rated voltage	415 V at 50 Hz
Rotor number of slots	24	CW rated current	5.3 A

III. Rotational Characteristics of the BDFIM Magnetic Fields

In order to assess the rotational behaviour of the flux density in the magnetic circuit of the BDFIM, the radial and tangential components of flux density (B_r and B_t respectively) in all the locations shown in Fig. 3 for stator and rotor iron are obtained for the prototype BDFIM by post processing of the non-linear FE model operating in synchronous mode and at rated operating conditions. The PW and CW supplied frequencies are set to be 50 Hz and 15 Hz, respectively resulting in the rotor speed of 650 rpm from (1) [18]:

$$n_r = \frac{f_1 + f_2}{p_1 + p_2} \tag{1}$$

The frequency of the rotor field can be obtained from [2]:

$$f_r = f_1 - p_1 \frac{n_r}{60} = f_2 - p_2 \frac{n_r}{60} \tag{2}$$

For the case when PW and CW frequencies are 50 Hz and 15 Hz, respectively, the rotor field frequency is therefore 28.33 Hz corresponding to a time period of approximately 35 ms.

The loci of flux density, B, at points P_1 to P_6 in the rotor iron shown in blue in Fig. 3 are obtained for three successive field cycles and shown in Fig 4. As shown, the B locis obtained for the three cycles at each point follow a similar rotating pattern. This confirms the periodic nature of the rotor field in the BDFIM with its frequency determined by (2) in synchronous mode of operation.

Kochmann in [19] proposed an analytical method for evaluating the rotating nature of the magnetic field by defining the ratio of the minor to the major axis of the flux density locus as shown in Fig. 5, called aspect ratio.

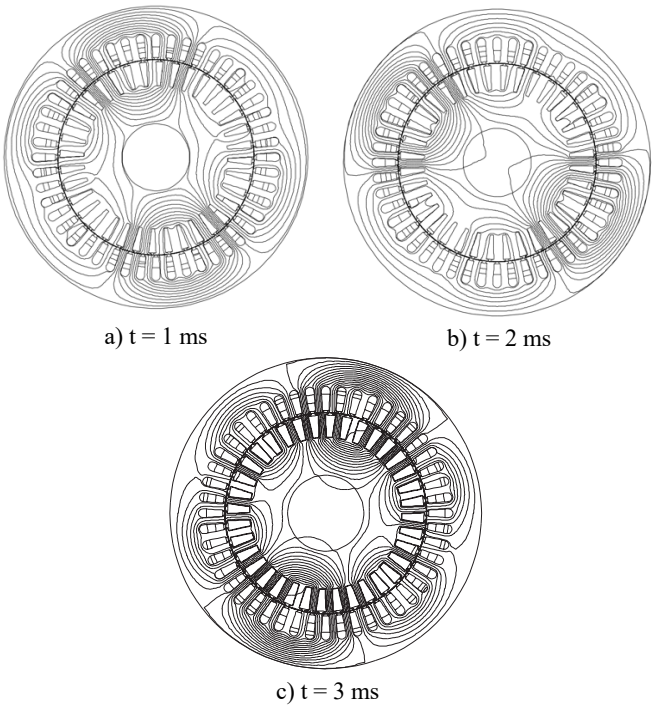

Fig. 2. Magnetic field pattern in the BDFIM iron for a) t = 1 ms, b) t = 2 ms, and c) t = 3 ms

Fig. 3. Locations on the stator (in red) and rotor (in blue) iron where the loci of flux density are obtained.

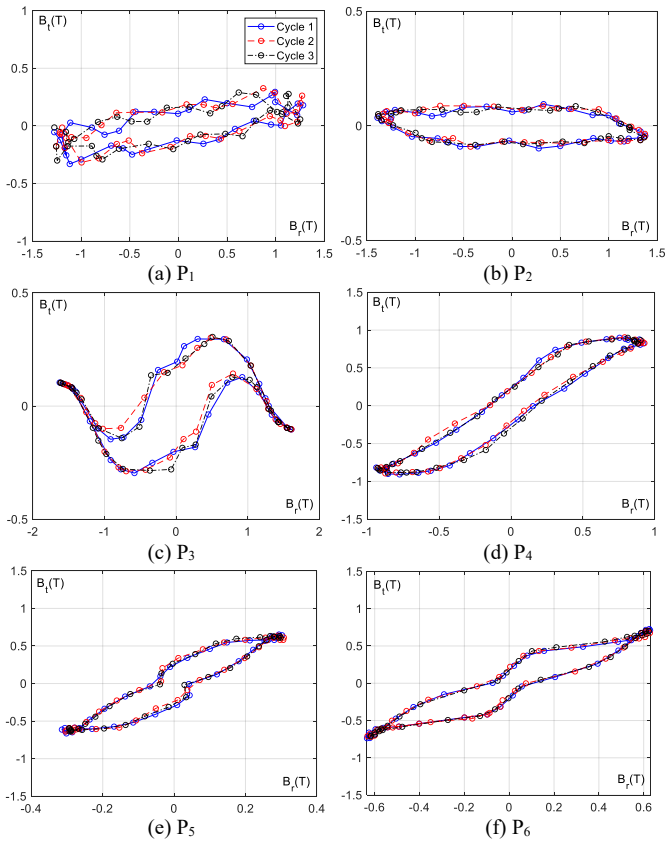

Fig. 4. Loci of B in the rotor iron. a) to f) correspond to points P_1 to P_6 specified in Fig. 3 in blue on the rotor iron, respectively.

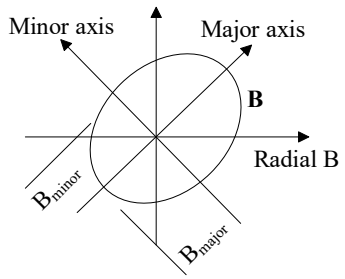

Fig. 5. A typical locus of B showing its minor and major axis components.

$$\lambda = \frac{|B_{minor}|}{|B_{major}|} \tag{3}$$

A value of zero corresponds to a pure alternating field; and the closer the ratio is to 1, the more the nature of flux density is rotational. The flux density along the minor and major axis, and the aspect ratio for the points specified in Fig. 3 are determined and shown in Table II. For rotor iron, the region close to the rotor surface (P_1) presents the largest ratio between the minor and major axes. This is because the stator and rotor tooth tip regions usually form the path for the high pole number slotting field harmonics which their pole numbers are related to the stator and rotor slot numbers. These harmonics tend to "zig-zag" along the stator/rotor air-gap interface leading to rotational field excitation. The behavior of the field along the rotor tooth and also at rotor back iron is nevertheless fairly alternative.

The stator rotational field pattern is more complex than the rotor since in the BDFIM stator the resultant field is the superposition of two magnetic fields induced by the stator windings with different magnitudes and supplied frequencies. With the operating conditions indicated in Section III i.e. 50 Hz and 15 Hz, for f_1 and f_2 respectively, the frequency of the resultant field will be equal to the greatest common factor of the stator frequencies, i.e. 5 Hz, corresponding to a time period of 200 ms for the stator field.

To assess the rotational characteristics of the magnetic field in the stator, the loci of flux density in the stator iron and for the points P_1 to P_6 shown in Fig. 3 in red are obtained for several successive 200 ms periods and shown in Fig. 6. In the stator iron, the region at the base of the stator tooth i.e. P_3 shows the most significant rotational behaviour with the back iron being next in importance. The flux density along the tooth body is almost alternating as expected. The only rotational components found in the tooth are in tooth tip region e.g. P_1 due to the leakage flux around the phase coils.

One important observation from Fig. 6 is that unlike the rotor iron, the B loci in none of the points in the stator iron follow a specific pattern in a way a single aspect ratio can be determined for each point. In order to further investigate the behaviour of the B loci in the stator iron, the B loci for two of the stator points i.e. P_3 and P_6 are decomposed into three sub B locis each is obtained from considering one cycle of the CW magnetic field (i.e. $1/15Hz = 66.7\ ms$).

TABLE II
FLUX DENSITY ALONG MINOR AND MAJOR AXIS IN THE ROTOR IRON

Points	B_{minor} (T)	B_{major} (T)	λ_s
P_1	0.36	1.31	0.27
P_2	0.11	1.41	0.08
P_3	0.83	1.21	0.69
P_4	0.69	1.36	0.51
P_5	0.48	1.44	0.33
P_6	0.18	1.32	0.14

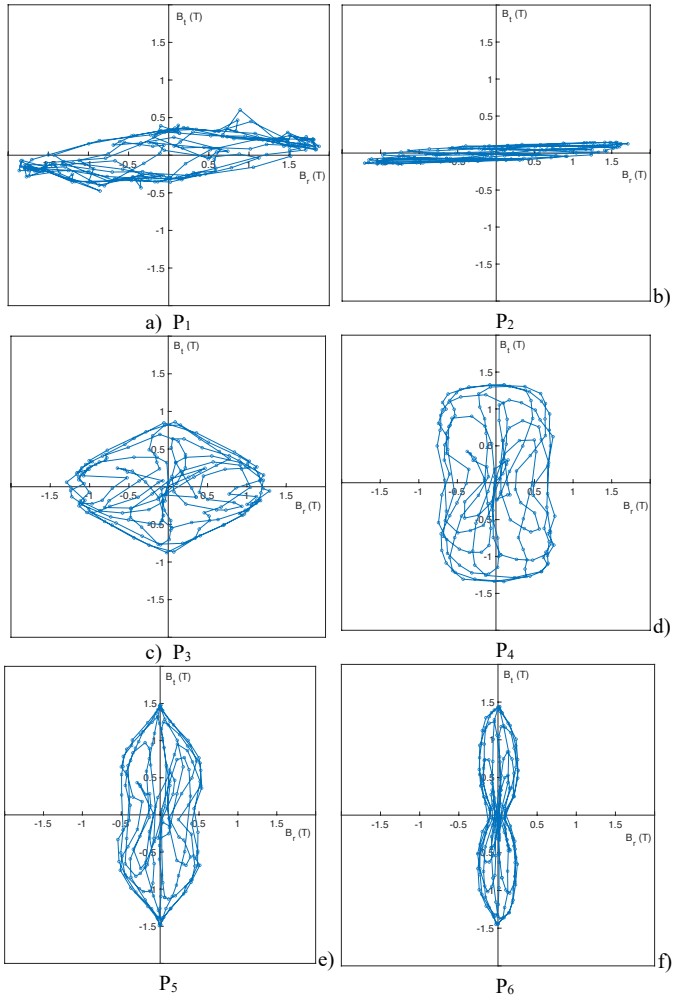

Fig. 6. Loci of B at points P_1 to P_6 indicated in Fig. 3 in red.

The results are shown in Figs. 7 and 8 for P_3 and P_6, respectively. It can be seen that for each CW cycle the B-loci will contain one major loop (loop 1) and several minor loops (loops 2 and 3). Loop 1 is common in all three CW cycles and hence is the dominant loop representing the main rotational characteristics of the field. However, the location and shape of the minor loops differ in each CW cycles and hence it is not possible to assign a single aspect ratio to each element of the stator iron.

Fig. 9 shows the time variation of the radial and tangential flux density components for stator iron elements P_1 to P_6 shown in Fig. 3. As clear, excessive higher order harmonics can be seen in both radial and tangential components of the flux density at various stator iron locations. Fig. 10 shows the Fast Fourier Transform (FFT) of the radial and tangential flux density for P_1 to P_6. As can be seen, the dominant frequencies are 50 Hz and 15 Hz corresponding to the stator PW and CW supplied frequencies, respectively.

Other higher order harmonic field components have shown to have large magnitudes that make the stator field significantly distorted. The presence of two fundamental field components as well as the other large higher order harmonics makes the conventional methods for single field machines not applicable for the BDFIM stator iron loss calculation.

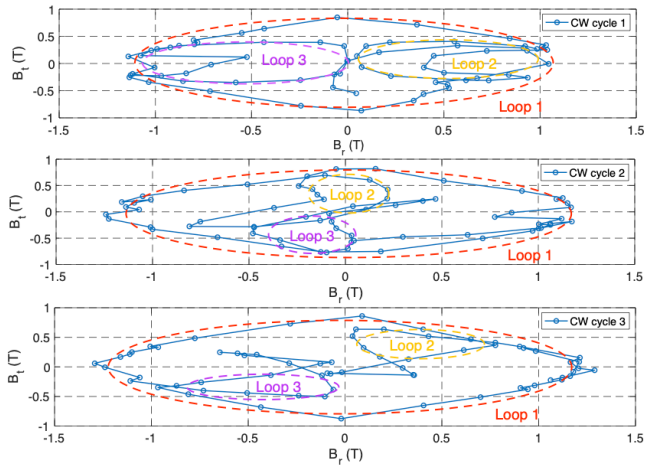

Fig. 7. Decomposition of B Loci at points P_3 into three CW cycles

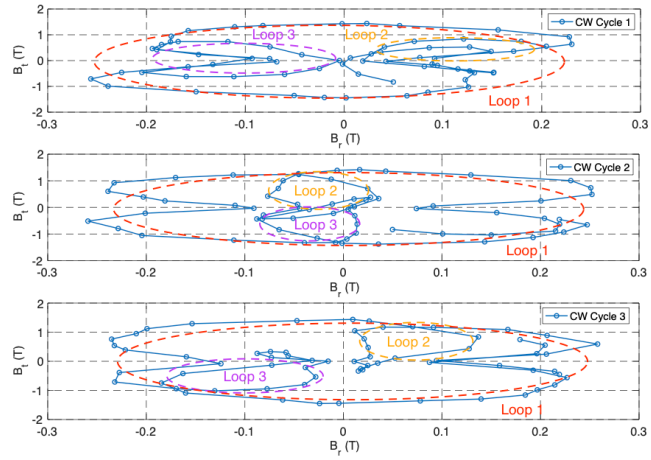

Fig. 8. Decomposition of B Loci at points P_6 into three CW cycles

IV. BDFIM Rotational Iron Loss Calculation

A. Hysteresis Loss Formulation

Zhu et al. in [20] developed a formula for hysteresis loss in electrical machines with elliptical flux density pattern:

$$P_{hyst} = P_{r-h}\lambda + (1-\lambda)^2 P_{alt-h} \quad (4)$$

where $\lambda = B_{minor}/B_{major}$ is the axis ratio of the elliptical B locus. $P_{r\text{-}h}$ and $P_{alt\text{-}h}$ are the iron losses with a circular B and an alternating B with $B_{major} = B_{peak}$, respectively, and B_{peak} is the peak value of the alternating B.

Equation (4) is used in this study to calculate the losses in the BDFIM's rotor iron taking the effects of the rotational fields into account. However, as discussed in Section III, the stator magnetic field has a complex pattern containing two fundamental field components with different frequencies, as well as the higher order harmonics with large magnitudes.

Equation (4) is independent of the magnetisation frequency since it is directly derived from the rotational iron loss formulation. Therefore, (4) is applicable to hysteresis loss calculation at any frequency.

A series of elliptical harmonic flux density vectors are obtained when the flux density in an element is expanded into its Fourier series. B_{minor} and B_{major} for the kth harmonic vector can be determined by a coordinate rotation for the standard equation.

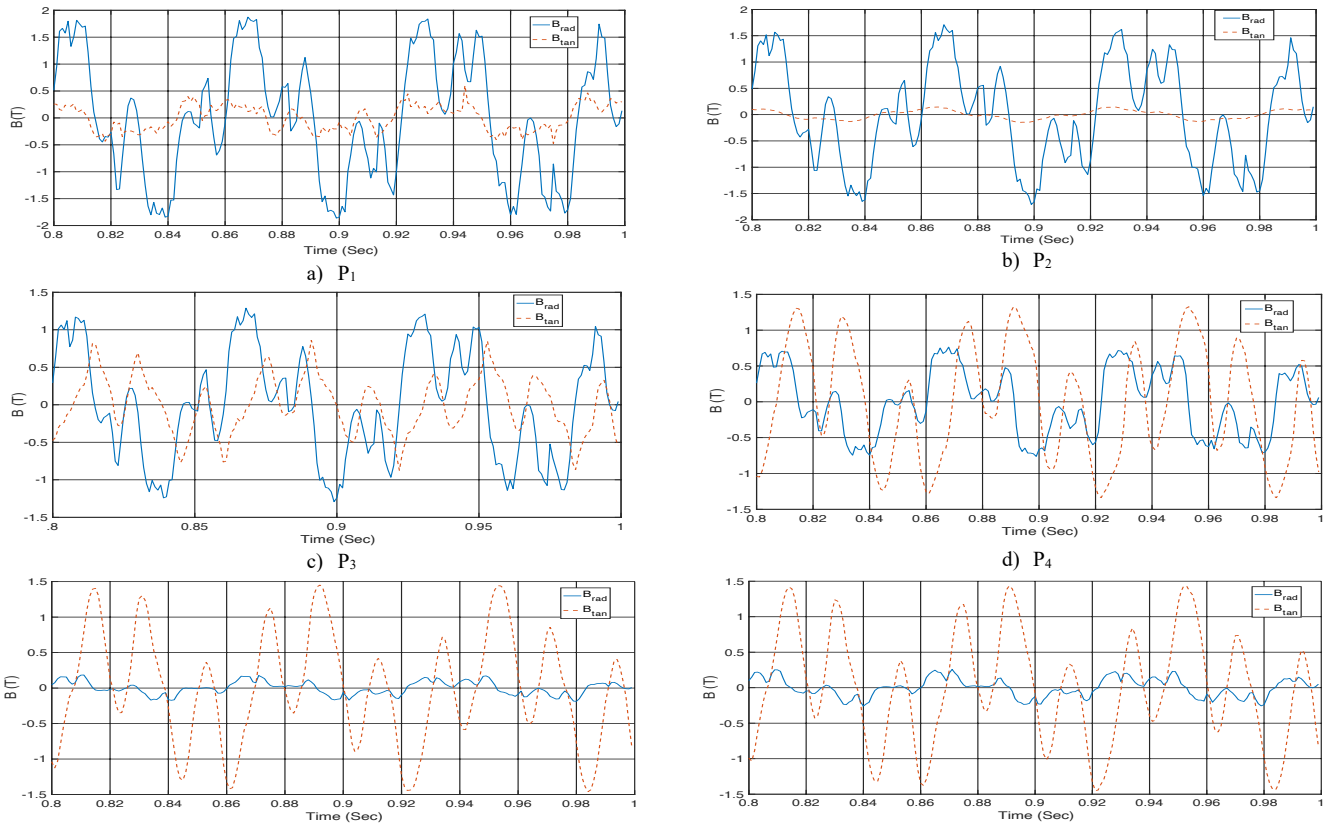

a) P_1 b) P_2 c) P_3 d) P_4 e) P_5 f) P_6

Fig. 9: Time variation of radial and tangential components of flux density: a) to f) correspond to points P_1 to P_6 indicated in Fig. 3 in the stator iron.

The total hysteresis loss in an element can then be obtained by summing up the contributions from these harmonics. For each harmonic, the hysteresis loss is predicted from the corresponding alternating and rotational hysteresis losses according to the axis ratio of the elliptical flux density by (3). Therefore, the total hysteresis loss is

$$P_{hyst-st} = \sum_{k=1}^{n} P_{r-hk}\lambda_K + (1-\lambda_K)^2 P_{alt-hk} \tag{5}$$

where $\lambda_k = B_{k-minor}/B_{k-major}$ is the aspect ratio of k_{th} harmonic flux density, $P_{r\text{-}hk}$ and $P_{alt\text{-}hk}$ are the rotational and alternating hysteresis losses with flux density $B_{k\text{-major}}$, obtained by Steinmetz law.

$$P_h = k_{hyst} k f B_{k-major}^2 \tag{6}$$

B. *Eddy-Current and Excess Loss Formulation*

The total rotational eddy-current loss in a rotor element can be obtained from [21]:

$$P_{e-rotor} = k_e \frac{1}{T}\int \left[\left(\frac{\partial B_r}{\partial t}\right)^2 + \left(\frac{\partial B_t}{\partial t}\right)^2\right] dt \tag{7}$$

The stator elemental eddy-current loss is obtained from the classical formulation and by summing up the effects of the rotational harmonic fields:

$$P_{e-stator} = K_e \sum_{k=0}^{\infty} (kf)^2 \left({B_{k-major}}^2 + {B_{k-minor}}^2\right) \tag{8}$$

In the presence of rotational magnetic field in the iron circuit, (7) can be used for calculation of the excess loss in both stator and rotor elements:

$$P_{ex} = k_{ex} \frac{1}{T}\int \left[\left(\frac{\partial B_r}{\partial t}\right)^2 + \left(\frac{\partial B_t}{\partial t}\right)^2\right]^{3/4} dt \tag{9}$$

C. *Computation of the BDFIM Iron Losses*

The specific iron loss data for the BDFIM lamination with type M530-65A were obtained from Epstein frame loss measurements, where the sample under test is subjected to sinusoidal excitation on the primary winding, while the open-circuit voltage on the secondary is measured [22].

The measured specific core losses for a frequency range of 10-50 Hz and flux densities from 0.5 to 2 T are shown in Fig. 11. The iron loss coefficients have then been deduced using the least square method by comparing the Epstein experimental loss data with (4) using the target function (10).

$$min\left(\sum_{f=f_1}^{fm}\sum_{B=B_1}^{Bn}\left[\frac{P_{loss-cal-f-B} - P_{loss-exp-f-B}}{P_{loss-exp-f-B}}\right]^2\right) \tag{10}$$

where $[f_1 - f_m]$ and $[B_1 - B_n]$ represent the frequency and flux density ranges the Epstein tests are carried out, and $P_{loss-cal-f-B}$ and $P_{loss-exp-f-B}$ are the calculated iron loss using (4) and the iron loss from Epstein test, respectively, at frequency f and flux density B.

The iron loss coefficients have been obtained for the BDFIM lamination M530-65A for two different cases of $B < 1.2\ T$ and $B > 1.2\ T$ so the resultant iron loss formulation of (4) can represent the lamination iron more accurately. The coefficient values are given in Table III.

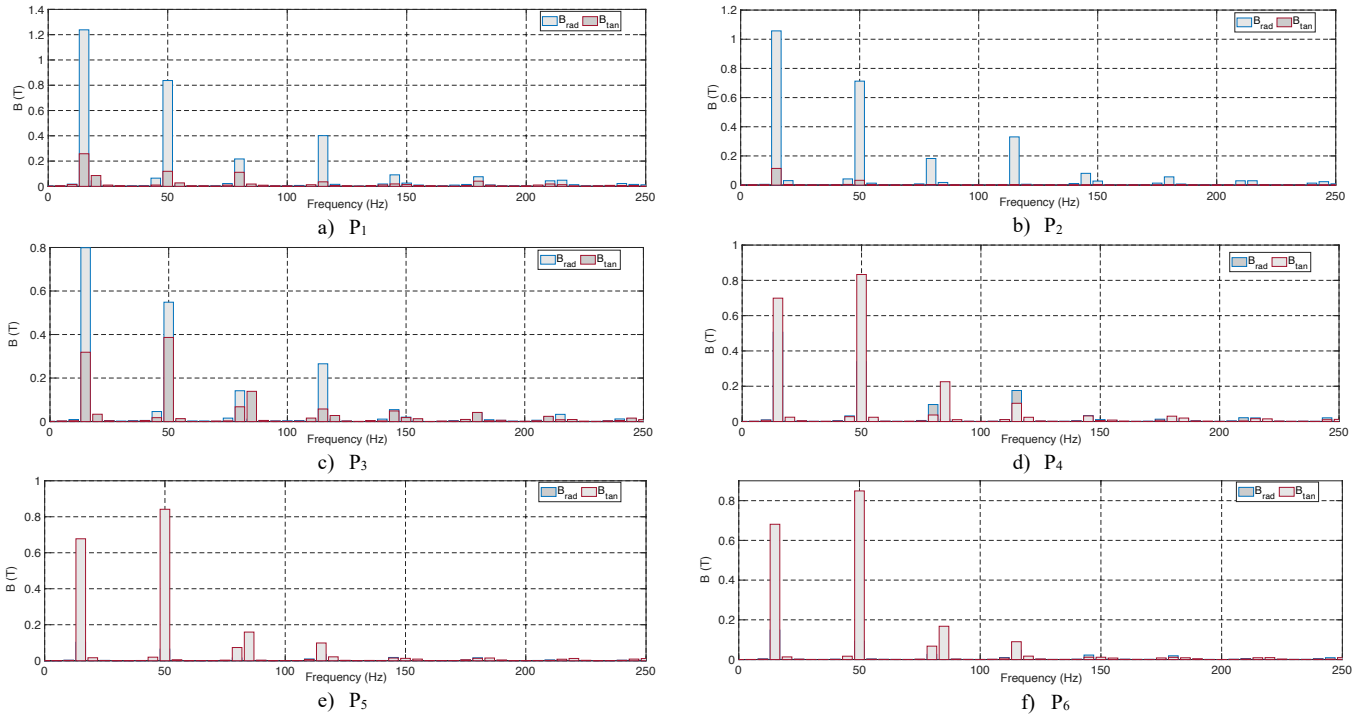

Fig. 10: Higher order time harmonics in radial and tangential components of the magnetic fields: a) to f) correspond to P_1 to P_6 in the stator iron in Fig. 3.

The 2-D FE time-stepping analysis is performed using a commercial software application EFFE [9] to compute the flux density in the stator and rotor iron circuits in synchronous mode of operation. Lumped parameters are used to incorporate the end region leakage effects into the analysis. The modelling takes into account the nonlinear properties of the iron for accurate analysis.

In order to validate the proposed iron loss computation method, an open-circuited rotor is used. Thus, the total iron losses can be obtained from no-load locked-rotor tests using stator winding measurements since both mechanical and rotor copper losses are eliminated. In this configuration, the total iron loss can be obtained by subtracting the stator cupper losses from the measured input power when the machine operates at no-load and locked-rotor condition.

$$P_{iron} = P_{in} - P_{cu-PW} - P_{cu-CW} \tag{11}$$

P_{in} is the total input power to stator PW and CW and the $P_{cu\text{-}PW}$ and $P_{cu\text{-}CW}$ are the copper losses dissipated in the stator PW and CW, respectively. Once the FE model is solved, the local flux density waveforms for both the stator and rotor regions are extracted from the FE solution. The flux density data for every element in the mesh at each time-step is logged in a file for further analysis.

The process is incremented to the next time-step and repeated until the required data for a complete period of the flux density is obtained. The data is then processed to obtain the radial and tangential components of the flux density, enabling the losses resulting from rotational flux patterns in the stator and rotor laminations to be calculated.

TABLE III
IRON LOSS COEFFICIENT VALUES OBTAINED FROM EPSTEIN FRAME TESTS

	k_e	k_{ex}	k_{hyst}
B < 1.2 T	0.00025	0.0019	0.0132
B > 1.2 T	0.00017	0.0012	0.0149

Next, the local loss densities are calculated using (5) to (10), then summed to give the elemental iron loss density. These iron loss densities are multiplied by the mass of the iron calculated using the element areas and length of the iron core.

Finally, these localised iron losses are summed to give the total iron loss dissipated in the machine.

V. EXPERIMENTAL VERIFICATION

Fig. 12 compares the iron losses computed from the proposed loss prediction formulation (4) to (9) with experimental results at different CW voltages. Close agreement can be seen between the computational results and experimental measurements which validates the practicality of the proposed iron loss modelling approach for the BDFM. The rise in the iron losses as the CW voltage is increased is due to the increase in the CW supply frequency set by the v/f controller.

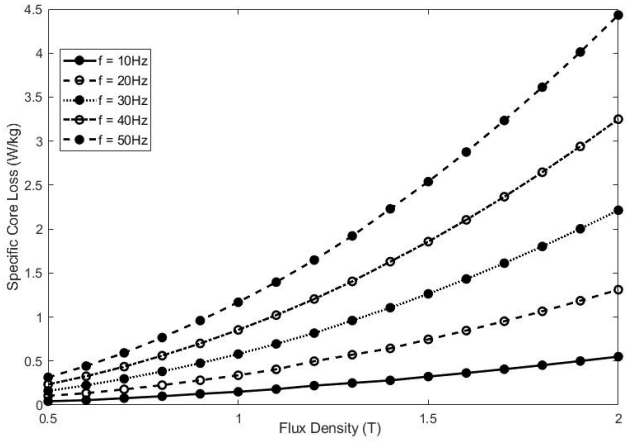

Fig. 11. Specific core loss data for the BDFIM lamination obtained from Epstein frame experiment.

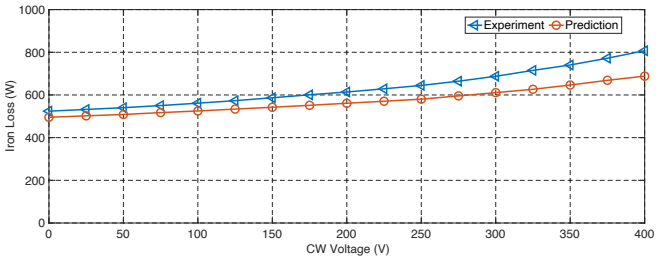

Fig. 12: Comparison of the proposed iron loss prediction results with experimental tests at various CW voltages.

Future work may include more accurate measurement of iron losses using calorimetric measurements and the thermal modelling of the machine for further optimisation of the thermal design. In addition, by utilising a wireless rotor current measurement technique, iron losses may be measured at more practical operating conditions, especially when the machine is loaded.

VI. Conclusions

In this paper, the magnetic field in the BDFIM stator and rotor iron have been studied with special focus on rotational behaviour of the field in the machine. It has been shown that in several locations of the stator and rotor iron the field has rotational characteristics that need to be taken into account in iron loss calculations. It has also been shown that the stator magnetic field in a BDFIM is complex since it contains two fundamental field components with different frequencies, magnitudes and pole numbers, as well as the additional higher order harmonics which their magnitudes cannot be ignored. This leads to the fact that the conventional rotational iron loss formulations cannot be applied to the stator loss calculation. A harmonic analysis of the stator magnetic field has been performed based on Fourier transform, and the elliptical form of the flux density at each harmonic frequency has been used to propose a modified formulation for the stator iron loss prediction. It has been shown experimentally using the open rotor winding configuration that the proposed iron loss formulation can predict the losses in the machine with acceptable accuracy.

VII. References

[1] S. Abdi, E. Abdi, A. Oraee, R. McMahon, "Investigation of magnetic wedge effects in large-scale BDFMs," *IET Renewable Power Generation Conference*, Beijing, China, September, 2013.

[2] S. Abdi, D. Liano, E. Abdi, P. Malliband, R. McMahon, "Experimental analysis of noise and vibration for large brushless doubly fed machines," *IET The Journal of Engineering*, Vol. 2017, pp. 724 - 728, 2017.

[3] N. Patin, E. Monmasson, J. Louis, "Analysis and control of a cascaded doubly-fed induction generator," in *Proc. 31st IECON*, vol. 30, pp. 2487–2492, Nov. 2005.

[4] S. Abdi, A. Oraee, E. Abdi, R. McMahon, "A new optimized rotor design for brushless doubly fed machines," *International Conference on Electrical Machines and Systems (ICEMS)*, August 2017.

[5] R. McMahon, P. Roberts, M. Tatlow, E. Abdi, A. Broekhof, S. Abdi, "Rotor parameter determination for the brushless doubly fed machine," *IET Electric Power Application*, vol. 9, pp. 549 - 555, 2015.

[6] A. Oraee, E. Abdi, S. Abdi, R. McMahon, P. Tavner, "Effects of rotor winding structure on the BDFM equivalent circuit parameters," *IEEE Transactions on Energy Conversion*, Vol. 30, pp. 1660 - 1669, 2015.

[7] R. Carlson, H. Voltolini, F. Runcos, P. Kuo-Peng, and N. Baristela, "Performance analysis with power factor compensation of a 75 kw brushless doubly fed induction generator prototype. " *IEEE International Conference on Electric Machines and Drives*, 2010.

[8] H. Liu and L. Xu, "Design and performance analysis of a doubly excited brushless machine for wind power generator application," *IEEE International Symposium on Power Electronics for Distributed Generation Systems*, pp. 597 – 601, 2010.

[9] S. Abdi, E. Abdi, R. McMahon, "Experimental and finite element studies of a 250 kW brushless doubly fed induction generator," *IET The Journal of Engineering*, vol. 2019, pp. 8489 – 8495, 2019.

[10] J. Chen, X. Wang, T. Zhao, Z. Li, M. Kong, P. Nie, "Application of brushless doubly-fed machine system in hydropower generation," *22nd International Conference on Electrical Machines and Systems (ICEMS)*, China, 2019.

[11] S. Abdi, E. Abdi, R. McMahon, "A light-weight rotor design for brushless doubly fed machines," *XIII International Conference on Electrical Machines*, Greece, 2018.

[12] F. Shibata and K. Taka. "Speed control for brushless cascade induction motors in control range of slips $s_1>1$ and $s_2>1$, " *IEEE Transactions on Energy Conversion*, vol. 2. pp. 246–253, June 1987.

[13] M. Ahmadian, B. Jandaghi, H. Oraee, "Hysteresis loss in brushless doubly fed induction machines", *The International Conference on Renewable Energies and Power Quality*, pp. 975-980, May 2011.

[14] A. Ferreira, S. Williamson, "Time-stepping finite-element analysis of brushless doubly fed machine taking iron loss and saturation into account", *IEEE Transactions on Industry Applications*, vol 35, No. 3, pp. 583-588, May 1999.

[15] F. Zhang, S. Yu, Y. Wang, S. Jin, M. Jovanovic, "Design and Performance Comparisons of Brushless Doubly-Fed Generators with Different Rotor Structures", *IEEE Transactions on Industrial Electronics*, vol. 66, pp. 631-640, January 2019.

[16] M. Hashemnia, F. Tahami, E. Oyarbide, "Investigation of core loss effect on steady-state characteristics of inverter fed brushless doubly fed machines", *IEEE Transactions on Energy Conversion*, vol. 29, No. 1, pp. 57-64, March 2014.

[17] S. Abdi, E. Abdi, A. Oraee, R. McMahon, "Optimization of magnetic circuit for brushless doubly fed machines," *IEEE Transactions on Energy Conversion*, vol. 30, pp. 1611 - 1620, 2015.

[18] S. Abdi, E. Abdi, H. Toshani, R. McMahon, "Vibration analysis of brushless doubly fed machines in the presence of rotor eccentricity," *IEEE Transactions on Energy Conversion*, vol. 35, No. 3, pp. 1372-1380, September 2020.

[19] T. Kochmann, "Relationship between rotational and alternating losses in electrical steel sheets," *Journal of Magnetism and Magnetic Materials*., vol. 160, pp. 145 - 146, July 1996.

[20] J. G. Zhu, V. S. Ramsden, "Core loss modelling in rotational electrical machines," *International Conference on Electrical Machines in Australia (ICEMA)*, Australia, 1993.

[21] S. Abdi, E. Abdi, R. McMahon, "A new iron loss model for brushless doubly fed machines with hysteresis and field rotational losses," *IEEE Transactions on Energy Conversion*, vol. 36, no. 4, December 2021.

[22] J, Geisinger, A. Knight "Investigation of iron losses in mixed frequency flux density waveforms", *IEEE Transactions on Magnetics*, vol. 50, no. 11, November 2014.

VIII. Biographies

S. Abdi received the B.Sc. degree in electrical engineering from Ferdowsi University, Mashhad, Iran, in 2009, the M.Sc. degree in electrical engineering from the Sharif University of Technology, Tehran, Iran, in 2011, and the Ph.D. degree in electrical machines design and optimisation from Cambridge University, Cambridge, U.K., in 2015. He is currently an Assistant Professor of electrical engineering with the University of East Anglia, Norwich, U.K. His main research interests include electrical machines and drives for renewable power generation and automotive applications.

E. Abdi (M'05–SM'12) received the B.Sc. degree in in electrical engineering from the Sharif University of Technology, in Iran, in 2002. He graduated from Cambridge University with the M.Phil. and Ph.D. degrees in electrical engineering, in 2003 and 2006, respectively. He is the Founder and Director of Wind Technologies Limited with Cambridge, where he has led the commercialisation of the brushless doubly-fed machine for wind power applications. His main research interests include electrical machines and drives, wind power generation, and electrical measurements and instrumentation.

H. Toshani received the B.Sc. degree in electrical engineering from the Ferdowsi University of Mashhad, Mashhad, Iran, in 2009 and the M.Sc. and Ph.D. degrees in control engineering from Iran University of Science and Technology, Tehran, Iran, in 2012 and 2021, respectively. He is currently a PDRA in the Engineering Department of Cambridge University, UK. His research interests include control theory, embedded systems, fault diagnosis of electrical machines and optimization techniques.